Progress In Electromagnetics Research, PIER 86, 71–86, 2008

A NOVEL MICROSTRIP PATCH ANTENNA WITH REDUCED SURFACE WAVE EXCITATION

S. F. Mahmoud and A. R. Al-Ajmi

EE Department
Kuwait University
P. O. Box 5969, Safat 13060, Kuwait

Abstract—A microstrip circular patch antenna with two shorting pins is proposed as an antenna with reduced surface wave and lateral wave excitation. Theoretical analysis of the cavity modes of the patch lead to a design procedure for the antenna. Simulation results using the IE3D-Zeland software support the theory and verify the reduced surface wave capability. By using four shorting pins instead of two, we demonstrate the possibility of achieving circular polarization with high polarization purity in addition to the reduced surface wave. It is demonstrated that a discrimination against the lateral wave of 30 dB or more is achievable. Applications include design of large patch arrays with reduced coupling and GPS receiving antennas that reduce low angle interfering signals.

1. INTRODUCTION

One of the major concerns in microstrip antenna design is the excited surface waves. In addition to their contribution to power loss, surface waves cause undesired coupling between components printed on the same substrate, such as the case in patch antenna arrays [1]. Several attempts have been made recently to reduce such coupling [e.g., 2–5]. Eventually, excited surface waves will be diffracted at the edges of a finite ground, which causes the radiation pattern to be corrupted and deviate from its desired shape. Besides, the presence of surface waves is usually associated with appreciable lateral waves and low angle radiation. This can introduce interfering signals in receiving antennas with broadside patterns such as the case with Global positioning system (GPS) and assisted GPS receiving antennas [6, 7].

It is well known that a circular patch antenna of radius 'a' operating in the dominant mode TM_{110} ($TM_{\phi\rho z}$) will resonate at a

frequency given by:

$$ka = x'_{11} = 1.8412 \tag{1}$$

where x'_{11} is the first root of the Bessel function derivative; $J'_1(x)$, and k is the wavenumber in the substrate medium. Meanwhile, it has been shown [8] that, in order to nullify the surface wave, the condition $\beta_{sw}a = 1.8412$ must be satisfied, where β_{sw} is the radial wavenumber of the dominant TM_{11} surface wave mode. When the dielectric substrate is electrically thin, as is usually the case, this is the only surface wave mode that can propagate and $\beta_{sw} \approx k_0$; k_0 being the wavenumber in air. Hence the condition for zero surface waves reduces to:

$$k_0 a = 1.8412 \tag{2}$$

Obviously, both conditions (1) and (2) cannot be simultaneously satisfied for non-air substrate. If we choose the radius 'a' to satisfy (2), the patch will not be resonant at the required frequency as clear from (1). So in order to nullify the surface wave and, at the same time have resonance at the specified frequency, some modification of the patch structure is needed. Notable work in this direction is given by Jackson and his team in [9, 10]. The patch is modified to become an annular ring [9] with shorted inner surface and outer open surface of radius 'a' given by (2). By adjusting the inner shorted radius, the ring can be made to resonate at the same frequency corresponding to (2). The short circuit is implemented by inserting a very high number of via pins between the patch and the ground. In another design the substrate is modified to have a smaller ε_r in an inner circular region of radius $c < a$ [11].

In this paper, we propose a simple design of a circular patch that can significantly reduce surface waves. Namely we consider a circular patch loaded with two shorting pins on a homogeneous grounded substrate as depicted in Fig. 1. The cavity mode analysis of this patch reveals that the mode which resembles the TM_{110} mode on the unloaded patch has a resonant frequency governed by:

$$ka > x'_{11} \tag{3}$$

The exact value of ka is a function of the pin position and radius. It is thus feasible to satisfy both (2) and (3) when the substrate ε_r is chosen properly. The one and two pin loaded circular patch has been treated earlier by one of the authors as a compact [12], multiband [13] and broadband [14] antenna for wireless applications. In the following section we review the derivation of the cavity modes of the patch in view of the surface wave reduction goal. Based on this study, a design procedure of a reduced surface wave patch antenna is given in Section 3.

Supporting simulation results based on the IE3D package is introduced in Section 4. We then turn attention to the design of an antenna with circular polarization. This calls for a patch with four shorting pins symmetrically placed on the patch. Analysis, design and simulation results are given in Section 5 and followed by concluding remarks.

2. CAVITY MODES OF A TWO-PIN SHORTED CIRCULAR PATCH

As demonstrated in Fig. 1, the patch has a radius 'a' and is shorted by two pins each of radius $b \ll a$ and located at (r_0, $\phi = +\alpha$) and (r_0, $\phi = -\alpha$) with respect to a cylindrical coordinate system with z axis coinciding with the patch axis. The substrate is of height 'h' and a relative permittivity 'ε_r'. According to the cavity model of the patch, the boundary $r = a$ is considered to behave as a magnetic wall. To derive the fields and the resonant frequencies of the normal modes, we start by assuming z-oriented currents $I_{1,2}\exp(j\omega_r t)$ flowing in the two pins, where ω_r is the (so far unknown) modal resonant frequency. For even modes (having E_z an even function of ϕ), we have $I_1 = I_2 = I$. Conversely, for odd modes, $I_1 = -I_2 = I$. Due to the smallness of the pins radii, the currents can be considered to be concentrated on the axes of the pins. The current density at $r = r_0$ can then take the form:

$$\begin{aligned} J_z(r,\phi) &= I/r_o\delta(r-r_o)\left[\delta(\phi-\alpha) \pm \delta(\phi+\alpha)\right] \\ &= 2I/\pi r_o\delta(r-r_o)\sum_{n=0}^{\infty}\chi_n\left[\begin{array}{c}\cos n\phi\cos n\alpha \\ \sin n\phi\sin n\alpha\end{array}\right] \end{aligned} \tag{4}$$

for even and odd modes respectively and $\chi_n = 1$ ($n \geq 1$) and $\chi_0 = 1/2$.

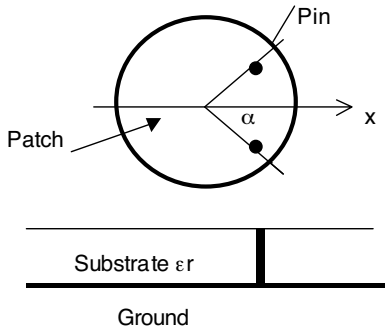

Figure 1. A circular patch of radius a with two shorting pins of radii b located at (r_0, $\pm\alpha$).

Following [13], and concentrating on even modes about x-axis, the modal electric field takes, for $0 \leq r \leq r_0$, the form:

$$E_z(r,\phi) = \sum_{n=0}^{\infty} C_n J_n(kr) \cos n\phi, \tag{5a}$$

and for $r_0 \leq r \leq a$,

$$E_z(r,\phi) = \sum_{n=0}^{\infty} C_n J_n(kr_0) \cos n\phi \frac{J_n(kr)Y_n'(ka) - Y_n(kr)J_n'(ka)}{J_n(kr_0)Y_n'(ka) - Y_n(kr_0)J_n'(ka)}, \tag{5b}$$

where $J_n(.)$ and $Y_n(.)$ are the Bessel functions of first and second kind; the prime denotes differentiation with respect to the argument and $k = \omega_r\sqrt{\varepsilon_r}/c$, with c the wave velocity in free space. It is noted that E_z is readily continuous at $r = r_0$, while $\partial E_z/\partial r = 0$ at $r = a$ satisfying the boundary condition at the magnetic wall. C_n's are constants to be determined from the discontinuity of $H_\phi = (1/j\omega\mu)\partial E_z/\partial r$ by the pin currents and are obtained as:

$$C_n = -j\omega\mu_0 I\chi_n \cos n\alpha \, \frac{J_n(kr_0)\, Y_n'(ka) - J_n'(ka)\, Y_n(kr_0)}{J_n'(ka)} \tag{6}$$

The modal equation for the normalized resonant frequency ka is obtained by imposing the boundary condition of vanishing E_z at the pin surface. After some manipulations, involving the addition theorem of the Bessel function [15, Sec. 5.8], we get:

$$Y_0(kb) \pm Y_0(kd) - 4\sum_{n=0}^{\infty} \chi_n \cos^2 \alpha J_n(k(r_0 - b) J_n(kr_0) Y_n'(ka)/J_n'(ka) = 0 \tag{7}$$

where d is the distance between the two pins. Of particular interest is the aperture E_z at $r = a$ which is the source of radiation and surface wave fields. Using (5b) and (6)

$$E_z(r = a, \phi) = \sum_{n=0}^{\infty} E_n \cos n\phi \tag{8}$$

where:

$$E_n = -2j\omega\mu I\chi_n \cos n\alpha \frac{J_n(kr_0)}{\pi k a J_n'(ka)} \tag{9}$$

The modal Equation (7) is solved numerically for the normalized resonant frequencies (ka) of the modes. The first three modes, in

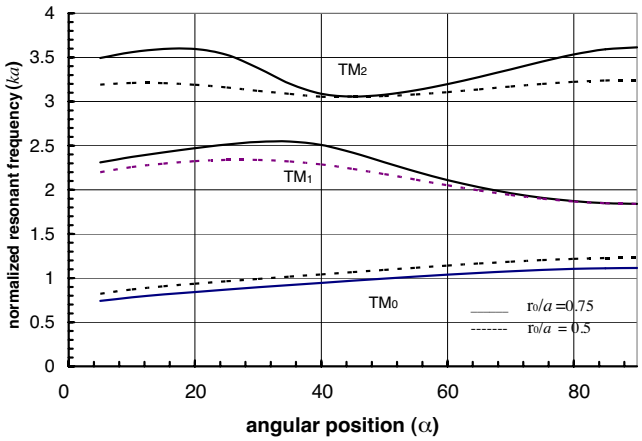

Figure 2. ka of the first three modes versus pin angular position α. b/a is fixed at 0.03.

the order of increasing ka, are plotted versus pin's angular position 'α' in Fig. 2.

A word about the labeling of these modes is in order. The modes are TM (to z) with no z-variation. The azimuthal variation is not a simple cos or $\sin(n\phi)$, but rather a weighted sum of harmonics as given by (5). So a given mode cannot be labeled as TM_{nm0} as is the case for unloaded circular patch. We will simply label the modes as TM_{m0}, where $m = 0, 1, 2, \ldots$, thus the modes are TM_{00}, TM_{10}, TM_{20}, ..., etc. A mode with a given 'm' will have a certain set of coefficients (E_n, $n = 0, 1, \ldots$) given by (9). It turns out that the TM_{m0} mode has the $|E_m|$ as the dominant coefficient, being greater than all other coefficients. This is true, at least, for the first 4 or 5 modes. In the following we shall further drop the subscript '0' (for z-variation) from the TM_{m0} modes to become simply TM_m modes.

Table 1. Aperture azimuth coefficients. ($b/a = 0.03$, $r_0/a = 0.7$).

$\mathbf{TM}_m$ **mode** m	α°	$\boldsymbol{E}_0$	$\boldsymbol{E}_1$	$\boldsymbol{E}_2$	$\boldsymbol{E}_3$
0	35°	**3.038**	−2.134	−0.254	0.0854
1	35°	0.197	**0.989**	−0.437	0.0731
2	35°	0.031	0.203	**0.626**	0.049
1	45°	0.140	**0.663**	**0**	0.117

To check the weights of the azimuthal harmonics E_n for the various modes, these harmonics are tabulated for the first three modes in the first three rows of Table 1. Here $\alpha = 35°$, $r_0/a = 0.7$ and $b/a = 0.03$. It is clear that the maximum coefficient (in magnitude) for the TM_0, TM_1 and TM_2 modes are respectively E_0, E_1, and E_2. Thus we can claim that the mode TM_1 for the pin loaded patch corresponds to the mode TM_{11} of the unloaded patch, the mode TM_2 of the pin loaded patch corresponds to the mode TM_{21} of the unloaded patch and so on. The case $\alpha = 45°$ is important since the E_2 coefficient vanishes as is evident from (9). Thus the TM_1 mode will behave more as $\cos(\phi)$, resembling the TM_{11} mode of the unloaded patch.

The normalized resonant frequency ka of the TM_1 mode is plotted versus r_0/a for two values of b/a in Fig. 3. Such results will serve as necessary data for the design of a patch antenna.

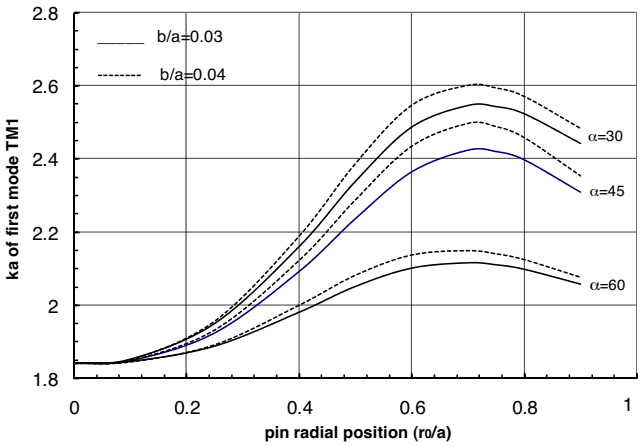

Figure 3. Normalized frequency ka of the TM_1 mode of a 2-pin loaded patch.

3. DESIGN OF A REDUCED SURFACE WAVE PATCH ANTENNA

The aperture E field given by (8)–(9) at $r = a$ is equivalent to a ring of magnetic current that excites both space waves and the surface wave mode TM_{11}, which is the only excited mode in view of the electrically small thickness of the substrate. The field of this surface wave mode

is derived in Appendix A and is given by:

$$E_{z,sw}(r,\phi,z) = \sum_{n=0}^{\infty} A_n J_n(\beta_s r) e^{-\gamma z} \cos n\phi \tag{10}$$

$$A_n = 2\chi_n \beta_s a E_n J_n'(\beta_s a) f(h,\varepsilon_r) \tag{11}$$

where β_s is the radial wavenumber of the surface wave mode. This formula is a generalization of that derived by Bhattacharyya [8] which is limited to n =1. Now as stated earlier, for the TM_1 mode of the present pin loaded patch, the E_1 term in the aperture field expansion is the dominant over all other E_n terms. So, if we choose $J_1'(\beta_s a) = 0$ (see (11)), a major reduction of the surface wave will be achieved. The residual surface wave power will be excited only by the weak E_n terms (with $n \neq 1$). This is the same condition required to nullify the surface wave on an unloaded patch, but we can also have the pin loaded patch resonate at the required frequency. Now a design procedure for our proposed patch can be outlined. For a given center frequency of interest, we use the condition of reduced surface wave in Equation (2) to determine the required patch radius a. The next step is to use the numerical results of ka, such as those in Fig. 3 to choose suitable pin positions and radii and the corresponding ka for the TM_1 mode. The corresponding relative permittivity ε_r of the substrate is computed as $\varepsilon_r = (ka/k_0 a)^2$. Practical values of ε_r can be obtained by proper choice of pin parameters r_0, b and α.

4. SIMULATION EXAMPLES

As a numerical example, we consider a patch antenna with pins' positions at ($r_o = 0.75a$, $\alpha = \pm 35^\circ$) and radii $b = 0.03a$. From (2), the patch radius is given by $a = 1.841\lambda_0/2\pi = 0.293\,\lambda_0$. From Fig. 3, we get $ka = 2.5479$, hence $\varepsilon_r = 1.918$. Using these data, the IE3D software is used to simulate the 2-pin shorted patch antenna and to plot the reflection loss; $\|S_{11}\|$ dB versus frequency in Fig. 4(a). The patch and the substrate are placed on a finite ground plane of 15 cm and the center frequency of the TM_1 mode is taken equal to 1.575 MHz (to simulate the L_1-band of the GPS) which corresponds to the second minimum of $\|S_{11}\|$ in Fig. 4(a) (the first minimum corresponds to the TM_0 mode). It is seen that the -10 dB bandwidth is approximately equal to 1.48% of the center frequency. The corresponding simulated gain pattern is plotted in both the E and H planes ($\phi = 0$ and 90 degrees) in Fig. 4(b). It is clear that the lateral wave level (at $\theta = 90^\circ$) is below the broadside radiation (along $\theta = 0^\circ$) by 40 dB in the E-plane, which proves the surface wave reduction design. However, the relative

lateral wave level jumps to -12 dB in the H-plane (y-z plane). This is attributed to the geometrical asymmetry about the y axis. The on-axis gain of the antenna is equal to 5.29 dB and the antenna efficiency (Prad/Pinput) is 85%.

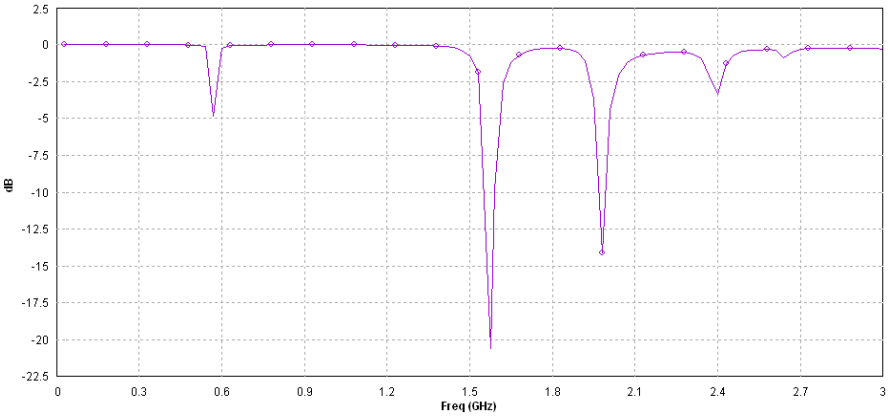

(a)

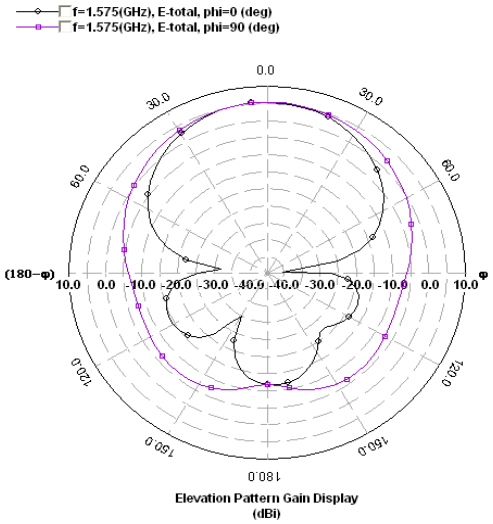

(b)

Figure 4. (a) Reflection loss (S_{11}) in dB versus frequency in GHz. $r_o = 0.75a$, $\alpha = \pm 35^\circ$ and $b/a = 0.03$. (b) Radiation pattern in both E and H planes. Same parameters as in Fig. 4(a).

Another example is shown in Fig. 5. Here $\alpha = 45°$, $r_0/a = 0.9$ and $b/a = 0.04$. The discrimination against the lateral wave, relative to the on-axis gain is 32 dB in the E-plane and 16 dB in the H-plane, which is somewhat better that the previous example where α was not equal to 45°.

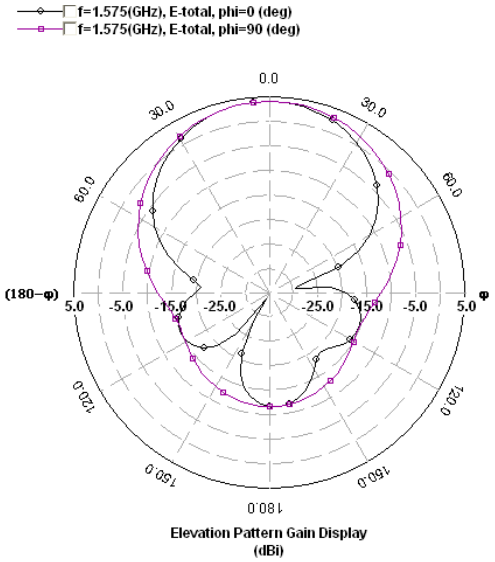

Figure 5. Radiation pattern in both E and H planes; $\alpha = \pm 45°$, $r_0/a = 0.9$ and $b/a = 0.04$.

5. CIRCULARLY POLARIZED PATCH ANTENNA WITH RSW

The patch antenna with two shorting pins considered above can produce linearly polarized radiation but is not suitable for circular polarization. This is so since the geometry lacks symmetry about the y-axis (the H-plane). In many applications, such as the GPS, circular polarization is the preferred polarization for combating space propagation effects [16, 17]. To radiate or receive such polarization, we propose a patch antenna with 4 shorting pins as depicted in Fig. 6. Here we choose $\alpha = 45°$ in order to get the same symmetry about x and y axes. The patch is fed by two feeds placed at $\phi = 0°$ and 90° and their currents are in phase quadrature.

To analyze this patch antenna, we follow the same steps as in Section 2 for the 2-pin shorted patch. However, we identify here 4

types of modes according to their even or odd symmetry about the x and y-axes. Namely, for the set of even/even modes, E_z is an even function of x and y, for the set of even/odd modes, E_z is an even function of x and odd function of y, and similar definition apply to the odd/even and odd/odd sets of modes. The modal equations for the even/even and even/odd sets of modes are derived in Appendix B and are given as:

$$Y_0(kb) + Y_0(kd_1) \pm Y_0(kd_2) \pm Y_0(kd_3) - 8 \sum_{n=even/odd}^{\infty} \chi_n \cos^2 \alpha J_n(k(r_0 - b) J_n(kr_0) Y_n'(ka)/J_n'(ka) = 0 \quad (12)$$

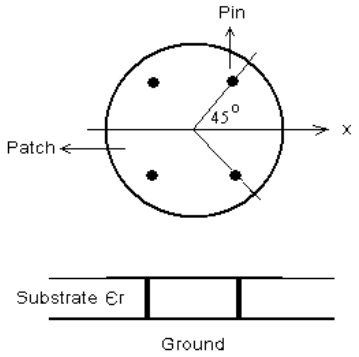

Figure 6. A circular patch of radius a with four shorting pins of radii b.

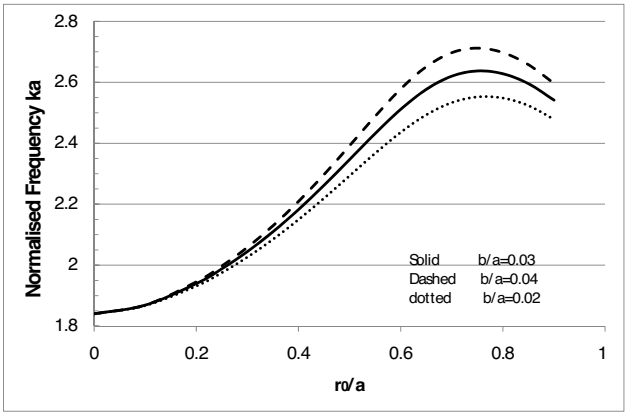

Figure 7. The normalized frequency TM_1 of the even/odd type of a 4-pin loaded circular patch.

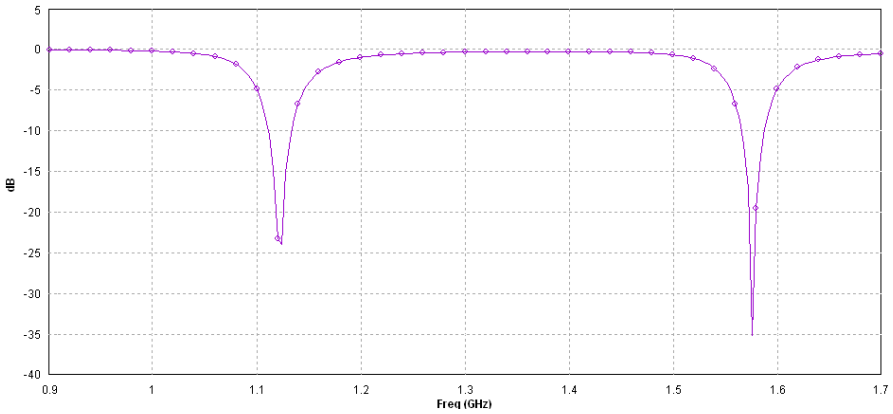

(a)

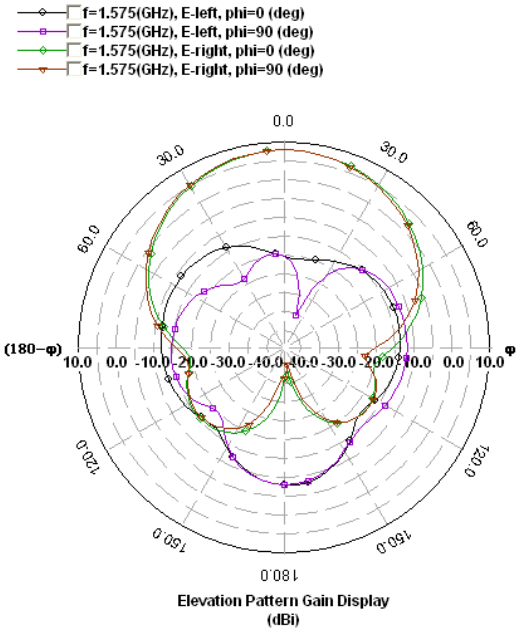

(b)

Figure 8. (a) Reflection loss (S_{11}) in dB versus frequency in GHz for a 4-pin shorted patch. $r_0/a = 0.7$ and $b/a = 0.03$. (b) Radiation pattern of the RHS and LHS polarization $\phi = 0$ and 90° planes. Same parameters as in Fig. 8(a).

The upper/lower labels apply to the even/even modes and the even/odd modes respectively. In (12), d_1, d_2, and d_3 are the distances to the pin at $\phi = +\alpha$ from the other three pins. Namely, $d_1 = 2r_0 \sin\alpha$, $d_2 = 2r_0 \cos\alpha$, and $d_3 = 2r_0$.

The aperture electric field, apart from a multiplying factor of two, is still given by Equations (8)–(9) except that the sum over n is limited to $n =$ even integers $(0, 2, \ldots)$ for the even/even modes and $n =$ odd integers $(1, 3, \ldots)$ for the even/odd modes. Thus the TM_1 mode of the even/odd type will be rich in the $\cos\phi$ armonic and hence will mostly resemble the TM_{11} mode of the unloaded circular patch. Therefore this mode is a candidate for reducing surface wave and lateral wave excitation when condition (2) is satisfied. The normalized resonant frequency ka of this mode is obtained by solving the modal Equation (12) for the first even/odd mode. The results are plotted for $\alpha = 45^\circ$ in Fig. 7 and can be used to design a circularly polarized patch antenna. For example, we choose $r_0/a = 0.7$ and $b/a = 0.03$ to get $ka = 2.62$, and since $k_0 a$ is forced to satisfy (2), we find that ε_r should have the value $\varepsilon_r = 2.02$.

We do a simulation of this 4-pin loaded patch at the GPS frequency of 1.575 GHz. The patch is fed by two feeds at $r_f = 0.43a$ and $\phi = 0$ and 90 degrees for right circular polarization. The results are given in Figs. 8(a) and (b). The reflection loss versus frequency (Fig. 8(a)) shows that the -10 dB bandwidth is 1.33% for the even/odd mode of interest. The gain patterns of the RHS (Copolar) and LHS (Crosspolar) polarizations in the $\phi = 0$ and 90° planes (Fig. 8(b)) shows a crosspolar discrimination better than 27 dB in both planes at the center frequency. The lateral wave is kept at a level of -30 dB relative to the on-axis copolar radiation in both $\phi = 0$ and 90° planes. Finally, in order to test the sensitivity of the design to change in the frequency, we change the frequency by +2% (1.6 GHz) and find that the increase in the lateral wave level is less than 2 dB (not shown).

6. CONCLUSIONS

A novel patch antenna with reduced surface wave and reduced lateral wave capability has been introduced. The antenna is composed of a circular patch with two shorting pins on a grounded dielectric substrate. By properly adjusting the patch radius, the pins' positions and the dielectric constant, one can achieve reduced surface wave at a prescribed resonant frequency. The idea is also extended to a 4-pin shorted patch where the pins are located at the angular positions $\phi = \pm 45^\circ$ and $\pm 135^\circ$. While the 2-pin patch can support only linearly polarized waves, the 4-pin patch supports circularly polarized waves

with high polarization purity and maintains the reduced surface wave property.

The cavity modes of the 2-pin and 4-pin shorted circular patch have been derived in detail and universal curves for the normalized resonant frequencies of the modes have been presented. Of particular interest is the mode which resembles the TM_{110} mode on unloaded circular patch. Design curves for the mode which resembles the TM_{110} mode on the unloaded patch are obtained. This mode can have the reduced surface wave property. The theory and the design procedure are supported by simulation examples obtained by using the IE3D software facility. Simulation results show that a circular polarization is achieved with crosspolar to copolar ratio of $-27\,\mathrm{dB}$ and $30\,\mathrm{dB}$ discrimination against the lateral wave. The results of this work should find applications in design of large patch antenna arrays and in GPS reception where surface waves and lateral waves need to be minimized.

APPENDIX A. APPENDIX AMPLITUDE OF SURFACE WAVE MODE

The aperture field of the patch E_z given in (8)–(9) is equivalent to a magnetic current ring mf that may be considered concentrated at the substrate-air interface at $z = 0$ where

$$m_\phi(a, \phi, 0) = E_z(a, \phi)h = \sum_{n=0}^{\infty} E_n h \cos n\phi, \tag{A1}$$

where E_n is given by (9). The surface wave mode excited by this source may be expressed as:

$$E_{z,sw}(r, \phi, z) = \sum_{n=0}^{\infty} A_n\, e_n(r, z) \cos n\phi, \tag{A2}$$

where:

$$\begin{aligned} e_n(r, z) &= J_n(\beta_s r) \exp\left(-\sqrt{\beta_s^2 - k_0^2}\, z\right); && z > 0 \\ &= J_n(\beta_s r) \cos k_z(z + h)/\varepsilon_r \cos k_z h; && -h \le z \le 0 \end{aligned}, \tag{A3}$$

where ε_r is the relative permittivity of the dielectric layer and $k_z = \sqrt{\varepsilon_r k_0^2 - \beta_s^2}$, and $k_0 = \omega\sqrt{\mu_0 \varepsilon_0}$ is the free space wavenumber.

The magnetic field associated with $e_n(r, z)$ is given by $h_{\phi,n}(r, z) = (j\omega\varepsilon/\beta_s^2)\, \partial e_n(r, z)/\partial r$. Now we use the reciprocity theorem [15]

between the field (A2) and its source (A1) and the source free field (A3) which results in A_n as:

$$A_n = \int_{\phi=0}^{2\pi} m_\phi h_{\phi,n}(a,0) a \cos n\phi d\phi \Big/ \int_{z=-h}^{\infty} \left(\pi\omega\varepsilon/\chi_n\beta_s^2\right) e_n^2(a,z)dz, \quad \text{(A4)}$$

which leads to Equations (10)–(11) in the text, with

$$f(h,\varepsilon_r) = \int_{z=0}^{\infty} \bar{e}_n^2(z)dz,$$

where $\bar{e}_n(z)$ has the same functional dependence on z as e_n of (A3).

APPENDIX B. CAVITY MODES ON A 4-PIN SHORTED CIRCULAR PATCH

Considering even/even modes, the pin currents are equal in the four pins, while the currents for the even/odd modes are $+I$ in the two pins at $\phi = \pm\alpha$ and $-I$ in the pins at $\phi = \pm(\pi - \alpha)$. Utilizing the result of Equation (4), we get the current density on the 4-pin loaded patch as

$$\begin{aligned} J_z(r,\phi) &= 2I/r_o\delta(r-r_o)\sum_{n=0}^{\infty}\chi_n\cos n\varphi(\cos n\alpha \pm \cos n(\pi-\alpha)) \\ &= 4I/\pi r_o\delta(r-r_o)\sum_{n=even/n=odd}^{\infty}\chi_n\cos n\varphi\cos n\alpha \end{aligned} \quad \text{(B1)}$$

The summation is over even values of n $(0, 2, 4\ldots)$ for the even/even set of modes and over odd values of n $(1, 3, \ldots)$ for the even/odd set of modes. Based on this equation, we get the modal electric field as in (5) after multiplying it by a factor of 2 and restricting the summation to even or odd integers depending on the set of modes considered. The same modifications should apply to the aperture field and the modal equation.

REFERENCES

1. Fallahi, R. and M. Roshandel, "Effect of mutual coupling and configuration of concentric circular array antenna on the signal to interference performance in CDMA systems," *Progress In Electromagnetics Research*, PIER 76, 427–447, 2007.

2. Suh, T. I., S. S. Lee, and H. T. Kim, "Mutual coupling reduction of antennas on a complex superstructure," *Journal of Electromagnetic Waves and Applications*, Vol. 18, No. 7, 983–991, 2004.
3. Zhu, Y.-Z., Y.-J. Xie, Z.-Y. Lie, and T. Dang, "A novel method of mutual coupling matching for array antenna design," *Journal of Electromagnetic Waves and Applications*, Vol. 21, No. 8, 1013–1014, 2007.
4. Ouyang, J., F. Yang, S. W. Yang, Z. P. Nie, and Z. Q. Zhao, "Non-surface wave mutual reduction in microstrip antennas array," *Journal of Electromagnetic Waves and Applications*, Vol. 22, No. 7, 915–922, 2008.
5. Kalaye, B. M. B. and J. Rashed-Mohassel, "A broadband and high isolation CPW fed microstrip antenna array," *Journal of Electromagnetic Waves and Applications*, Vol. 22, No. 2/3, 325–334, 2008.
6. Parkinson, B. W., *Global Positioning System: Theory and Application, (Volume One)*, Chapter 14, American Institute of Aeronautics & Ast, 1996.
7. Liew, S. C., K. G. Tan, and T. S. Lim, "Investigation of direct A-GPS positioning for hybrid E-OTD/GNSS," *Journal of Electromagnetic Waves and Applications*, Vol. 20, No. 1, 79–87, 2006.
8. Bhattacharyya, A. K., "Characteristics of space and surface-wave in a multilayered structure," *IEEE Transactions on Antenna and Propagation*, Vol. 38, 1231–1238, Aug. 1990.
9. Jakson, D. R., J. T. Williams, A. K. Bhattacharyya, R. L. Smith, S. J. Buchheit, and S. A. Long, "Microstrip patch that don not excite surface waves," *IEEE Transactions on Antenna and Propagation*, Vol. 41, No. 8, Aug. 1993.
10. Bassilio, L. I., J. T. Williams, D. R. Jackson, and M. A. Khayat, "A comparative study for a new GPS reduced surface wave antenna," *IEEE Antenna Wireless Propagation Letters*, Vol. 4, 2005.
11. Mehrotra, A. R., D. R. Jackson, J. T. Williams, and S. A. Long, "An annular-ring reduced surface wave microstrip antenna," *Antenna and Propagation Society International Symposium, 1999, IEEE*, Vol. 2, Aug. 1999.
12. Mahmoud, S. F. and R. K. Deep, "Characteristics of a circular microstrip patch antenna with a shorting post," *Journal of Electromagnetic Waves and Applications*, Vol. 16, No. 2, 213–226, 2002.

13. Mahmoud, S. F. and A. Almutairi, "A 2-pin loaded patch as a multiband antenna for wireless communication," *Applied Computer Electromagnetic Society Journal*, Nov. 2003.
14. Almutairi, A. F., S. F. Mahmoud, and N. A. Aljuhaishi, "Wideband circular patch antenna with 2-pins loading for wireless communications," *Journal of Electromagnetic Wave Applications*, Vol. 19, No. 6, 839–851, 2005.
15. Harrington, R. F., *Time Harmonic Electromagnetic Fields*, Sec. 5.8, McGraw Hill, 1961.
16. Sim, C. Y. D. and B. H. Yang, "A single layer dual band CP microstrip antenna for GPS and DSRC applications," *Journal of Electromagnetic Waves and Applications*, Vol. 22, No. 4, 529–539, 2008.
17. Wu, G.-L., W. Mu, G. Zhao, and Y.-C. Jiao, "A novel design of dual circularly polarized antenna fed by L-strip," *Progress In Electromagnetics Research*, PIER 79, 39–46, 2008.